Nanoscale precipitates as sustainable dislocation sources for enhanced ductility and high strength

Shenyou Peng[a,b], Yujie Wei[a,b,1], and Huajian Gao[c,d,1]

[a]The State Key Laboratory of Nonlinear Mechanics (LNM), Institute of Mechanics, Chinese Academy of Sciences, Beijing 100190, People's Republic of China; [b]School of Engineering Sciences, University of Chinese Academy of Sciences, Beijing 100049, China; [c]School of Mechanical and Aerospace Engineering, College of Engineering, Nanyang Technological University, Singapore 639798; and [d]Institute of High Performance Computing, Agency for Science, Technology and Research (A*STAR), Singapore 138632

Contributed by Huajian Gao, January 24, 2020 (sent for review August 23, 2019; reviewed by Scott X. Mao and Cem Tasan)

Traditionally, precipitates in a material are thought to serve as obstacles to dislocation glide and cause hardening of the material. This conventional wisdom, however, fails to explain recent discoveries of ultrahigh-strength and large-ductility materials with a high density of nanoscale precipitates, as obstacles to dislocation glide often lead to high stress concentration and even microcracks, a cause of progressive strain localization and the origin of the strength–ductility conflict. Here we reveal that nanoprecipitates provide a unique type of sustainable dislocation sources at sufficiently high stress, and that a dense dispersion of nanoprecipitates simultaneously serve as dislocation sources and obstacles, leading to a sustainable and self-hardening deformation mechanism for enhanced ductility and high strength. The condition to achieve sustainable dislocation nucleation from a nanoprecipitate is governed by the lattice mismatch between the precipitate and matrix, with stress comparable to the recently reported high strength in metals with large amount of nanoscale precipitates. It is also shown that the combination of Orowan's precipitate hardening model and our critical condition for dislocation nucleation at a nanoprecipitate immediately provides a criterion to select precipitate size and spacing in material design. The findings reported here thus may help establish a foundation for strength–ductility optimization through densely dispersed nanoprecipitates in multiple-element alloy systems.

nanoscale precipitate | dislocation sources | ductility | strength | multiple-element alloy

Recent experiments have shown that multiple-element alloys with nanoscale precipitates could effectively circumvent the well-known strength–ductility dilemma and achieve ultrahigh strength and large ductility (1–8). As nanoscale precipitates are thought to primarily act as obstacles to dislocation glide (9, 10), how they help achieve high strength without sacrificing ductility remains a puzzle. Obstacles to dislocation glide typically strengthen materials (9, 10) but are not necessarily beneficial to ductility. The development of dislocation pile-up in front of an obstacle often gives rise to stress concentrations and microcracking at high stress levels (11), and contributes to the long-standing strength–ductility conflict in engineering materials (12).

Among various strategies to overcome the conflict between strength and ductility in crystalline metals, the dominant one is to tune and manipulate dislocation activity (9, 10). Introducing gradient structures (13) and dual phase (14–16) are some of the strategies that have been utilized to enhance both strength and ductility. While precipitate hardening has been well established and widely employed in systems like aged Al–Cu alloys, Ni-based superalloys and maraging steels (17–19), it has also been recognized that misfitting particles can generate dislocations in a ductile matrix (20, 21). Experiments suggest stronger and more complex precipitate–dislocation interactions in materials with nanoscale precipitates (1, 22, 23) as well as dislocation nucleation at nanointerfaces (24–27). Motivated by the observed superior strength–ductility performance in alloys with nanoprecipitates (1–8) and dislocation nucleation from nanointerfaces (24–27), here we propose yet another strategy to achieve superb strength–ductility combination in alloys with densely dispersed nanoprecipitates which simultaneously serve as dislocation sources and obstacles, leading to a sustainable and self-hardening deformation mechanism for enhanced ductility and high strength. We show via atomistic simulations that nanoprecipitates are a unique type of sustainable dislocation sources at high stress.

Atomistic simulations were performed to investigate dislocation activities around a nanoscale precipitate in a crystallite matrix. The simulation materials and methods are detailed in *Materials and Methods*. In Fig. 1 *A* and *B*, we show, respectively, the evolution of shear stress, shear strain, and both potential and kinetic energies as a function of time when the precipitate–matrix system shown in Fig. 1*C* is subject to a shear strain. As seen in Fig. 1*A*, we first increased the strain at a constant rate until the first dislocation nucleation event, and then held the applied strain constant ($\varepsilon_{yz} = 5.6\%$). A slight stress drop is identified as a result of plastic deformation by dislocation nucleation and glide. Here only the resolved shear stress that contributes to dislocation motion is considered. In Fig. 1*B*, we see that several more dislocations are generated at constant ε_{yz} before the source is deactivated. The potential energy decreases due to dislocation-induced plasticity, while the kinetic energy increases as a consequence of plastic dissipation. Even after the stress is relaxed to a level which is insufficient to nucleate new dislocations, both the potential energy and stress continue to decrease due to the motion and interaction of existing dislocations, as seen in the dashed lines in Fig. 1 *A* and

Significance

Precipitates in a material are traditionally thought of as dislocation obstacles that lead to elevated strength and reduced ductility. In contrast, recent experiments suggest that nanoscale precipitates facilitate both high strength and large ductility. To help resolve this apparent paradox, here we reveal that nanoprecipitates provide a unique type of dislocation sources that are activated at sufficiently high stress levels and render uniform plasticity by simultaneously serving as efficient dislocation sources and obstacles to dislocation motion, giving rise to sustained deformability. The findings can guide development of next generation of materials such as multiple-element alloys with precipitate engineering.

Author contributions: Y.W. and H.G. designed research; S.P. and Y.W. performed research; S.P., Y.W., and H.G. analyzed data; and S.P., Y.W., and H.G. wrote the paper.

Reviewers: S.X.M., University of Pittsburgh; and C.T., Massachusetts Institute of Technology.

The authors declare no competing interest.

This open access article is distributed under Creative Commons Attribution-NonCommercial-NoDerivatives License 4.0 (CC BY-NC-ND).

[1]To whom correspondence may be addressed. Email: yujie_wei@lnm.imech.ac.cn or huajian.gao@ntu.edu.sg.

This article contains supporting information online at https://www.pnas.org/lookup/suppl/doi:10.1073/pnas.1914615117/-/DCSupplemental.

First published February 24, 2020.

Downloaded at Institute of Mechanics CAS on August 31, 2020

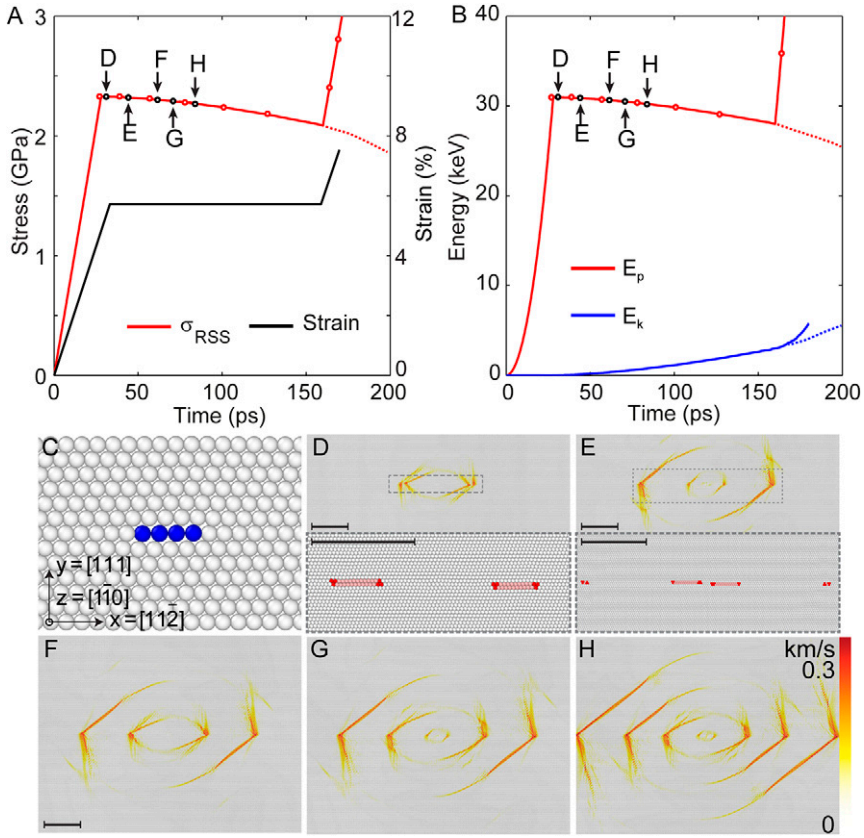

Fig. 1. Nucleation of screw dislocations at a nanoprecipitate. (*A*) The resolved shear stress (σ_{RSS})/applied strain (ε_{yz})–time curve. Each initial nucleation is indicated by the red circles, and dislocation nucleation events shown in *D–H* are keyed in black. (*B*) Potential-energy and kinetic-energy profiles during dislocation nucleation in response to shearing, where the black circles correspond to *D–H*. (*C*) The precipitate arrangement and the coordinate, where Cu atoms are shown in white and Au in blue; (*D–H*) Atomic velocity contours at stress or energy states indicated in *A* and *B*; The detailed atomic structures circled in *D* and *E* are also shown, with atoms colored by common neighbor analysis values. (Scale bar, 8 nm.)

B. The source can be repeatedly reactivated by increasing strain and stress to a sufficiently high level, and each subsequent activation requires increasingly higher stress, as shown in the solid black line in Fig. 1*A*. This behavior is referred to as self-hardening. In Fig. 1 *C–H*, we show the detailed atomic structure. A two-dimensional (2D) sample with a Au precipitate in an otherwise perfect face-centered cubic (FCC) crystal of Cu is shown in Fig. 1*C*. Due to the lattice mismatch between the precipitate and matrix, a local stress concentration arises and at a certain critical applied shear stress, dislocation pairs begin to nucleate and glide on the [111] plane (Fig. 1 *D–H*). The atomic velocity fields induced by the moving dislocations are shown for clarity. The respective stress and energy corresponding to each nucleation event shown in Fig. 1 *D–H* are indicated by the black circles in Fig. 1 *A* and *B*.

The nucleated screw dislocations are formed at the junction of the nanoprecipitate and matrix in response to the applied shear strain ε_{yz}. The nucleated dislocations soon become supersonic and move above the shear wave speeds (28), as can be clearly seen from the Mach cones in the atomic velocity contour in Fig. 1*E*. The detailed atomic structures during dislocation nucleation are presented at the bottom of Fig. 1 *D* and *E*.

The structural change accompanied by the nucleation processes is detailed in Fig. 2. The formation of leading partials at the two ends of the nanoprecipitate is shown in Fig. 2*A*. The extension of the leading partials gives rise to a wide stacking fault followed by a trailing partial (Fig. 2*B*). The leading partial–stacking fault–trailing partial structure of a full screw dislocation is then compressed (Fig. 2 *C–E*) as the dislocation moves at a supershear speed (28). After the dislocation moves away from the precipitate for some distance, another leading partial emerges from the nanoprecipitate and the nucleation process repeats (Fig. 2*F*). Repeated dislocation nucleation can be seen when the applied strain exceeds a critical level (Fig. 1 *A* and *B*), and these dislocation activities lead to a slight stress relaxation. The dynamics of dislocation nucleation is presented as a movie in Movie S1.

Following Peierls and Nabarro (29, 30), the displacement mismatch between neighboring layers characterizes the atomic feature of a dislocation core. A mismatch function ϕ is defined as $\phi = u/b$, where b is the magnitude of a unit Burgers vector (for FCC crystal, $\boldsymbol{b} = \frac{a}{2}\langle 110\rangle$ with lattice parameter a), u is the mismatch displacement, $u = u_z$ for screw dislocations, and $u = u_x$ for the edge dislocations. We show in Fig. 2 *G–L* the dislocation structures corresponding to different snapshots shown in Fig. 2 *A–F*. As both ends of the precipitate emit dislocations, we focus on the nucleation process at the right end (along the x axis). A generated full screw dislocation is composed of a leading partial and a trailing partial, the Burgers vectors of both having a screw component b_s and an edge component b_e, with magnitudes $b_e = b/\sqrt{12}$ and $b_s = b/2$.

Depending on the applied stress, the nucleated dislocation could be of the edge type as well. We demonstrate that under shear strain ε_{xz}, edge dislocation pairs are nucleated under sufficiently large deformation, as shown in *SI Appendix*, Fig. S1. Usually, higher critical stress is required for edge dislocation nucleation due to its greater energy barrier. For precipitates containing the same number of atoms, their shape can also play an important role in

Downloaded at Institute of Mechanics CAS on August 31, 2020

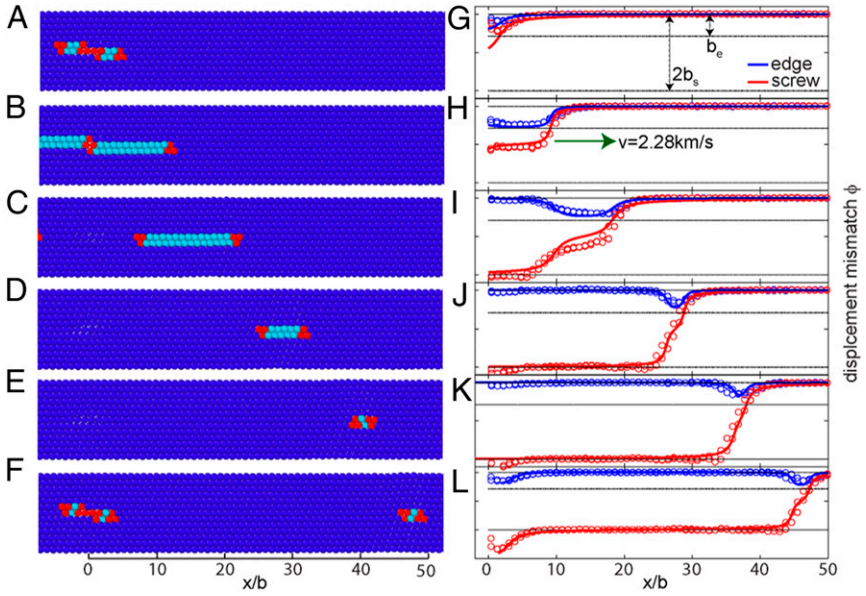

Fig. 2. The atomic and structural information of full screw dislocations nucleated from a nanoprecipitate. The *x* axis is normalized by the unit Burgers vector *b*. (*A*–*F*) The atomic information of the dislocation cores: (*A*) Initial nucleation with the formation of two leading partials at the two ends of the nanoprecipitate, and we track dislocations nucleated at the right end of the precipitate; (*B*) Extension of the nucleated leading partial to form stack faults; (*C*) Nucleation of a trailing partial to form a full screw dislocation at one end. (*D* and *E*) The compressed core of the full screw. (*F*) Another nucleation event from the nanoprecipitate. There can be multiple nucleations even though the applied strain is held constant. (*G*–*L*) The corresponding displacement mismatch of the nucleation core at different snapshots in accordance with *A*–*F*.

determining the critical stress for dislocation nucleation, which is demonstrated in detail in *SI Appendix*, Fig. S2.

Dislocation nucleation is robustly seen even for subnanometer-sized precipitates. Such dislocation source could be of great interest as a complementary mechanism for plasticity in high-strength alloys with nanoscale hard phases or heterogeneities (8, 16, 23, 31, 32), which seem to be an intrinsic feature of many alloy systems, in particular the emerging multielement alloys (33, 34). We consider a precipitate of 8 × 8 × 2 layers of Au embedded in an otherwise perfect FCC Cu crystal, as shown in Fig. 3*A*. We apply a gradually increasing shear strain ε_{yz} to the sample until the first nucleation event and then keep ε_{yz} constant afterward. The corresponding stress–time curve is shown in Fig. 3*B*. In Fig. 3 *C*–*H*, we present the configurations of dislocation loops nucleated from the precipitates keyed in Fig. 3*B*. Only atoms in the dislocation core are shown according to a color mapping based on their distance to the precipitate, with red ones close to but blue ones far away from the precipitate center. Typically, a leading partial with stacking fault is generated first and followed by a trailing partial. The velocity and shape of a dislocation line are dependent on crystallographic directions; see *SI Appendix*, Figs.S3 and S4. Dislocations are repeatedly nucleated after a critical strain is reached, accompanied with slight stress relaxation due to dislocation gliding-induced plasticity, as can be seen in the dynamic process shown in Movie S2.

The interfacial properties between the precipitate and matrix are affected by both the lattice misfit and the size of the precipitate. As the crystal structures of the two are the same and the precipitate is at nanoscale, the interface is rather strong and remains coherent after dislocation nucleation. Various simulations with different precipitate sizes are performed and similar results are observed. The strain when the first dislocation nucleates is precipitate-size dependent.

As nanoprecipitates could be an essential source of deformability for high-strength metals, the critical strain or stress level

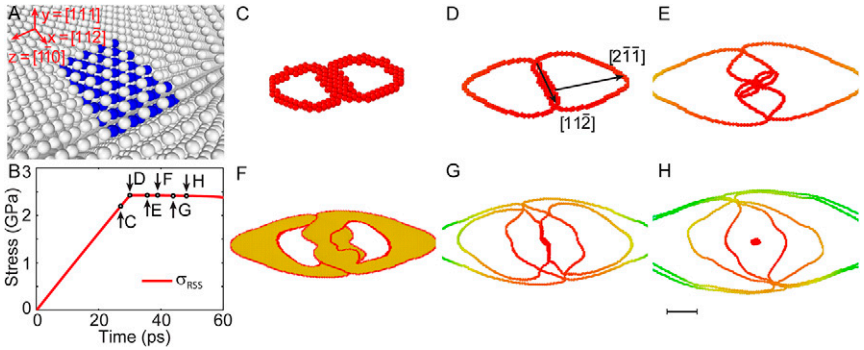

Fig. 3. Nucleation of dislocation loops at a subnanometer-sized precipitate. (*A*) The structure of the precipitate, with Cu atoms shown in white and Au in blue; (*B*) stress vs. time. Here we applied a constant shearing rate until point d and then kept the applied strain constant; (*C*–*H*) The nucleation and extension of dislocation loops at states keyed in *B*. (Scale bar, 6 nm.)

Downloaded at Institute of Mechanics CAS on August 31, 2020

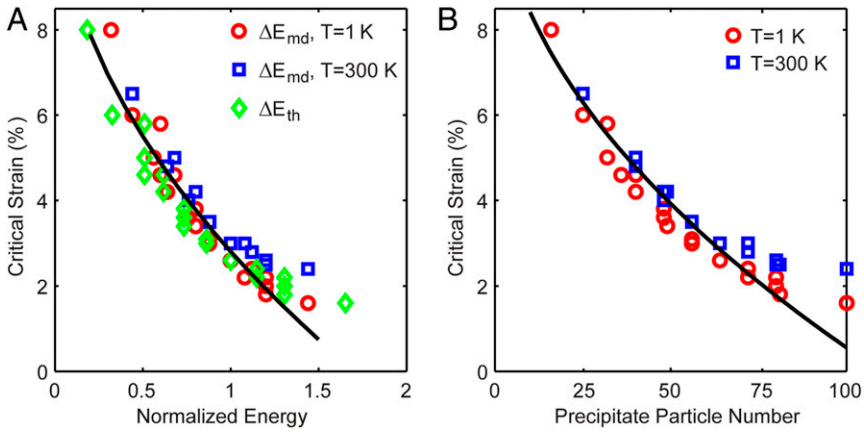

Fig. 4. The dependence of critical strain to trigger dislocation nucleation. (*A*) Relation between critical strain and distortion energy caused by nanoprecipitates. Here red circles denote the change of potential energy from 3D simulations. (*B*) Precipitate size dependence of the critical strain.

to attain nucleation is of interest. Based on the Peierls concept, Rice (35) proposed an energy criterion to analyze dislocation nucleation form a crack tip. Along this line, further analysis and simulation are performed here to predict the energy barrier for dislocation nucleation (36–39).

The lattice mismatch between the matrix and precipitate gives rise to a stress concentration, and hence lowers the barrier for dislocation nucleation. We explore the distortion energy caused by the precipitate by calculating the potential-energy difference between crystals with and without an embedded precipitate. This is denoted as ΔE_{md} and obtained directly from the molecular-dynamics (MD) simulations. The nanoprecipitates lower the potential energy of the system, here measured as the difference $\Delta E_{md} = E_0 - E_p$, where E_0 is the potential energy without any precipitate and E_p with the precipitate. Alternatively, we may treat the lattice misfit between the precipitate and matrix as a continuous distribution of infinitesimal dislocations, with total Burgers vector equal to the overall lattice mismatch. As detailed in *SI Appendix*, the strain energy due to the precipitate can be written as

$$\Delta E_{th} = \frac{Gb^2}{4\pi(1-\nu)}\left[\ln\left(\frac{R}{L}\right)+\frac{1}{2}\right], \qquad [1]$$

where b is the total Burgers vector of the smeared-out dislocations, R is the radius of the finite domain surrounding the precipitate, and L is the characteristic size of the precipitate. For a precipitate of (m,n,l) layers in the respective crystallographic direction defined in Fig. 3*A*, the total misfit b is $b = 2(m+n)(a_p - a_m)$, and a_p and a_m are the lattice constants of the precipitate and the matrix, respectively.

We combined our simulation results with different initial (m,n,l) in Fig. 4. In Fig. 4*A* the potential-energy difference (normalized for convenience) from simulations are shown as red circles, and the strain energy from equivalent dislocations are shown in green. All energy terms are normalized by the strain energy of a rectangular precipitate of $m = 8$, $n = 8$, $l = 2$. We see a clear relation between the distortion energy and the critical strain when dislocation nucleation begins, as seen by the fitting black line in Fig. 4*A*. The energy follows a quadratic dependence on the applied strain as $\Delta E_{md} = G(\varepsilon_c - \varepsilon)^2 V_0$, where $G = 46$ GPa is the shear modulus of Cu, $\varepsilon_c = 12\%$ is the elastic strain limit of the simulated Cu crystal, and V_0 is the activation volume for dislocation nucleation, ranging from $10b^3$ to $10^4 b^3$ according to different dislocation mechanisms (40). Here we use $V_0 = 10.2\ \text{nm}^3 = 600b^3$. In Fig. 4*B*, we show the size dependence of the critical strain for dislocation nucleation, where the size of the nanoprecipitate is defined as the number of Au atoms. The dependence could be fitted by $NE_a = G(\varepsilon_c - \varepsilon)^2 V_0$, with an average distortion energy density $E_a = 0.4$eV for a precipitate atom and N is the number of atoms in the precipitate. We recognize from Fig. 4*B* that larger precipitates require smaller strain to trigger dislocation nucleation, and the corresponding stress level is indeed comparable to that of recently reported high-strength metals with a large amount of nanoscale precipitates (2). In addition, simulations under $T = 300$ K show that a higher temperature causes a slightly greater critical strain, as seen from the blue circles in Fig. 4. It is pointed out that the strain of a small crystal can approach a very large value (nearly the theoretical elastic strain limit) (41–43), which justifies the use of nanoscale precipitates as effective dislocation sources.

For an alloys system with dense nanoprecipitates, we suggest two length scales which concurrently govern the strength and ductility of the material: the precipitate size d and precipitate spacing L.

Using Eshelby's inclusion solution (44), we may express the distortion energy of a misfit precipitate as $\Delta E \propto G\left(\frac{a_p - a_m}{a_m}\right)^2 d^3$, d being the equivalent precipitate diameter. Hence, we have $\alpha G\left(\frac{a_p - a_m}{a_m}\right)^2 d^3 = \frac{(\sigma_c - \sigma)^2}{G} V_0$, where α is a nondimensional parameter associated with precipitate shape and material property and σ_c the ideal strength. The stress to activate dislocation nucleation at a nanoprecipitate is then given as

$$\sigma = \sigma_c - \beta G\left(\frac{d}{b}\right)^{3/2}. \qquad [2]$$

We show in Fig. 5 the theory prediction (red curve) vs. experimental data for nanoprecipitate steels from literature (1, 2, 5) using $\beta = 6.0 \times 10^{-5}$, and $\sigma_c = 2.2$ GPa. The encouraging comparison between theory and experiments supports that nanoprecipitates play a key role in the superb strength–ductility combination of these materials. As nanoprecipitates facilitate dislocation nucleation at high stress, precipitate engineering may be particularly important for high-strength materials. For example, typical yield strength in maraging steels falls in the range of 1.0–2.0 GPa, where improved ductility was achieved (1–8) by aging treatment (45–47) with proper aging time, aging temperature, and precipitate fraction. In contrast, aged Al alloys and Ni-based superalloys do exhibit significant improvement in strength but so far lack reports on toughness enhancement.

Downloaded at Institute of Mechanics CAS on August 31, 2020

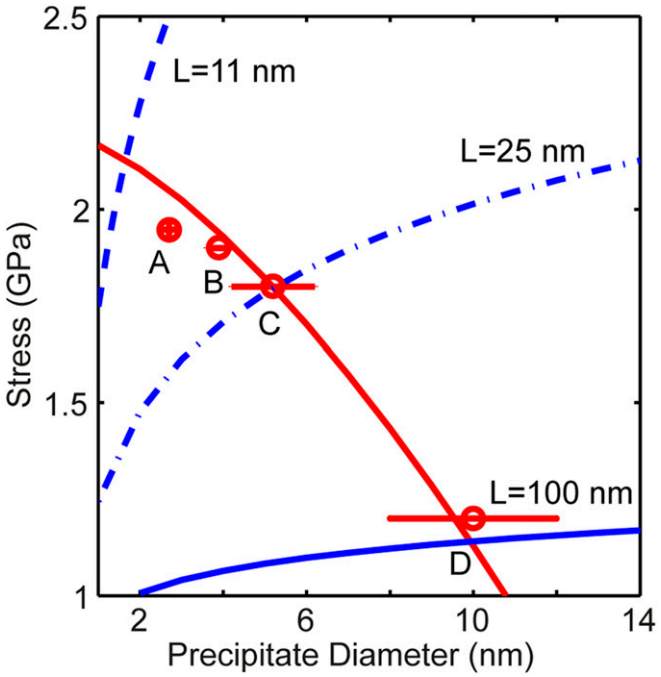

Fig. 5. The relation between strength and precipitate diameter in steels and proposed design guideline. Experimental data are adopted from Jiang et al. (2) (point A), Sun et al. (5) (points B and C), and Raabe (1) (Point D). The red line is predicted using Eq. **2**. The blue lines are predicted using Eq. **3**, with $L = 11$ nm for the dashed line, $L = 25$ nm for the dash-dotted line, and $L = 100$ nm for the solid line. The intersection points of blue lines and the red line indicate optimal precipitate sizes for strength–ductility combination.

On the other hand, the Orowan looping mechanism (5) for precipitate hardening predicts a strength increment $\Delta\sigma_{Or}$ as

$$\Delta\sigma_{Or} = 0.4M\frac{Gb}{\pi\sqrt{1-\nu}L}\ln\left(\frac{\sqrt{2/3}d}{b}\right), \qquad [3]$$

where $M \approx 3$ is the Taylor factor, $\nu \approx 0.34$ is the Poisson ratio, and L is the interparticle spacing. The overall yield strength is $\sigma = \sigma_0 + \Delta\sigma_{Or}$, σ_0 being the value in the absence of Orowan strengthening. By substituting $L = 11$ nm (2), $L = 25$ nm (5), $L = 100$ nm (1) into Eq. **3**, we obtain a relation between yield strength (with $\sigma_0 \approx 850$ MPa) and precipitate diameter as shown by the blue lines in Fig. 5.

Combining the Orowan strengthening effect and the softening effect from dislocation nucleation, one may obtain a preferred precipitate size at a given precipitate density (or a preferred precipitate density at a given precipitate size) that enhances the yield stress without the loss of ductility. The intersection point of blue lines and red line in Fig. 5 predicts the precipitate size and the corresponding attainable strength for a given precipitate spacing.

In summary, we have investigated dislocation nucleation caused by nanoscale precipitates using large-scale MD simulations. We found that, under sufficiently large shear strain, simultaneous dislocation nucleation and propagation will occur near a precipitate. Therefore, nanoscale precipitates provide a unique type of sustainable dislocation sources which differ fundamentally from the traditional Frank–Read source in crystalline materials. In contrast to the widely held perception that nanoprecipitates act as highly efficient obstacles to dislocation motion, thereby enhancing the strength of the material, our results demonstrate that nanoprecipitates can also be a sustainable dislocation source. Densely dispersed nanoprecipitates simultaneously serve as dislocation sources and obstacles, with both deformability and local hardenability to achieve enhanced ductility, which explains the unexpectedly high ductility of recently reported advanced alloys (1–8).

It is worth noting that most existing observations on the effects of precipitates on dislocation activities were focused on dislocation interaction, rather than dislocation nucleation. Typical in situ experiments with thin samples inside a transmission electron microscope do not involve sufficiently high stress levels to trigger dislocation nucleation from a precipitate before failure. Precipitates in a highly confined environment, such as precipitate containing micro/nanopillars subjected to compression, may provide a clean platform to validate the mechanism under study.

Combined with Orowan's precipitate hardening model, our energy-based criterion for dislocation nucleation at a nanoprecipitate can be employed to guide the design of high-strength materials with good ductility, as we demonstrated in Fig. 5 for steels with nanoscale precipitates. We emphasize that the small precipitate size of nanoscale precipitates leads to sustainable dislocation nucleation at high stress, and their coherent interface with matrix facilitates improved ductility. The generated dislocations interact with neighboring precipitates, and the related hardening scenario is consistent with the classic precipitate–dislocation interaction mechanism. As a consequence, the energy or stress to activate more dislocations of the same type has to increase resulting in local hardening. A dense distribution of such sources thus renders uniform deformation and better ductility. Our study suggests that the interplay of the two length scales, precipitate size and spacing, can be utilized as an optimal design motif for superb strength–ductility combination. This finding may help establish a foundation for tuning and optimizing strength–ductility performance in alloys with nanoprecipitates.

Materials and Methods

MD simulations are employed to investigate the dislocation nucleation induced by nanoprecipitates in FCC copper. All simulations are performed in the large-scale atomic/molecular massively parallel simulator (48). The embedded atom method potential (49, 50) is used to capture the atomic interaction between precipitate of Au and perfect FCC single crystal of Cu. The dimensions of periodic simulation boxes are about (530, 187, 0.8 nm) and (66, 51, 25 nm) for 2D and three dimensional (3D) simulations, respectively.

Since a full dislocation in FCC crystal glides at [111] plane and along its Burgers vector ⟨110⟩, we set x, y, z coordinates of the simulation box parallel to $[11\bar{2}]$, [111], $[1\bar{1}0]$ crystallographic directions, respectively. By replacing a number of Cu atoms with Au atoms, we obtain a sample with nanoprecipitates and the FCC structure remains. After energy minimization and structure relaxation, we apply shear strain ε_{yz} at a constant strain rate of 2×10^9 s^{-1} to the sample under the microcanonical ensemble for constant atoms (N), volume (V), and energy (E). Once dislocations start to nucleate, we stop increasing the applied strain and keep it constant. Initial temperature of $T \approx 1$ K and $T \approx 300$ K are employed in our simulation to verify the temperature influence. As the atomic structure changes when the dislocation nucleation occurs, we trace the nucleation process by the common neighbor analysis values of nucleated atoms. The critical nucleation state can also be obtained by counting the distorted atoms.

SI Appendix is available in the online version of the paper.

Data Availability Statement. All data are available in the main text and *SI Appendix*.

ACKNOWLEDGMENTS. Y.W. acknowledges support from the National Natural Science Foundation of China (NSFC) Basic Science Center for "Multiscale Problems in Nonlinear Mechanics" (Grant 11988102), as well as NSFC Grants 11425211 and 11790291; the Strategic Priority Research Program of the Chinese Academy of Sciences (CAS) (Grant XDB22020200), and CAS Center for Excellence in Complex System Mechanics. H.G. acknowledges support from the National Science Foundation through Grant DMR-1709318 to Brown University. The simulations are conducted at the Supercomputing Center of CAS. The authors are also very grateful to Shawn A. Chester at New Jersey Institute of Technology for valuable discussion and proofreading.

Downloaded at Institute of Mechanics CAS on August 31, 2020

1. D. Raabe, D. Ponge, O. Dmitrieva, B. Sander, Nanoprecipitate-hardened 1.5 GPa steels with unexpected high ductility. *Scr. Mater.* **60**, 1141–1144 (2009).
2. S. Jiang *et al*., Ultrastrong steel via minimal lattice misfit and high-density nanoprecipitation. *Nature* **544**, 460–464 (2017).
3. J. Y. He *et al*., A precipitation-hardened high-entropy alloy with outstanding tensile properties. *Acta Mater.* **102**, 187–196 (2016).
4. Y. L. Zhao *et al*., Development of high-strength Co-free high-entropy alloys hardened by nanosized precipitates. *Scr. Mater.* **148**, 51–55 (2018).
5. L. Sun *et al*., A novel ultra-high strength maraging steel with balanced ductility and creep resistance achieved by nanoscale β-NiAl and Laves phase precipitates. *Acta Mater.* **149**, 285–301 (2018).
6. Z. Fu *et al*., A high-entropy alloy with hierarchical nanoprecipitates and ultrahigh strength. *Sci. Adv.* **4**, eaat8712 (2018).
7. K. Ming, X. Bi, J. Wang, Realizing strength-ductility combination of coarse-grained Al0.2Co1.5CrFeNi1.5Ti0.3 alloy via nano-sized, coherent precipitates. *Int. J. Plast.* **100**, 177–191 (2018).
8. S.-H. Kim, H. Kim, N. J. Kim, Brittle intermetallic compound makes ultrastrong low-density steel with large ductility. *Nature* **518**, 77–79 (2015).
9. A. Argon, *Strengthening Mechanisms in Crystal Plasticity* (Oxford University Press, 2007).
10. P. M. Anderson, J. P. Hirth, J. Lothe, *Theory of Dislocations* (Cambridge University Press, ed. 3, 2017).
11. J. Weertman, *Dislocation Based Fracture Mechanics* (World Scientific, Singapore, 1996).
12. R. O. Ritchie, The conflicts between strength and toughness. *Nat. Mater.* **10**, 817–822 (2011).
13. T. H. Fang, W. L. Li, N. R. Tao, K. Lu, Revealing extraordinary intrinsic tensile plasticity in gradient nano-grained copper. *Science* **331**, 1587–1590 (2011).
14. X. Wu *et al*., Heterogeneous lamella structure unites ultrafine-grain strength with coarse-grain ductility. *Proc. Natl. Acad. Sci. U.S.A.* **112**, 14501–14505 (2015).
15. E. Ma, Eight routes to improve the tensile ductility of bulk nanostructured metals and alloys. *JOM* **58**, 49–53 (2006).
16. G. Wu, K.-C. Chan, L. Zhu, L. Sun, J. Lu, Dual-phase nanostructuring as a route to high-strength magnesium alloys. *Nature* **545**, 80–83 (2017).
17. E. Nembach, G. Neite, Precipitation hardening of superalloys by ordered γ′-particles. *Prog. Mater. Sci.* **29**, 177–319 (1985).
18. A. Ardell, Precipitation hardening. *Metall. Trans. A Phys. Metall. Mater. Sci.* **16**, 2131–2165 (1985).
19. T. Gladman, Precipitation hardening in metals. *Mater. Sci. Technol.* **15**, 30–36 (1999).
20. M. Ashby, L. Johnson, On the generation of dislocations at misfitting particles in a ductile matrix. *Philos. Mag.* **20**, 1009–1022 (1969).
21. T. Tan, W. Tice, Oxygen precipitation and the generation of dislocations in silicon. *Philo. Mag.: J. Theor. Exp. Appl. Phys.* **34**, 615–631 (1976).
22. D. N. Seidman, E. A. Marquis, D. C. Dunand, Precipitation strengthening at ambient and elevated temperatures of heat-treatable Al(Sc) alloys. *Acta Mater.* **50**, 4021–4035 (2002).
23. Z. Li, C. C. Tasan, H. Springer, B. Gault, D. Raabe, Interstitial atoms enable joint twinning and transformation induced plasticity in strong and ductile high-entropy alloys. *Sci. Rep.* **7**, 40704 (2017).
24. X. Liao *et al*., Deformation mechanism in nanocrystalline Al: Partial dislocation slip. *Appl. Phys. Lett.* **83**, 632–634 (2003).
25. L. Wang, Z. Zhang, E. Ma, X. Han, Transmission electron microscopy observations of dislocation annihilation and storage in nanograins. *Appl. Phys. Lett.* **98**, 051905 (2011).
26. S. Zheng *et al*., Deformation twinning mechanisms from bimetal interfaces as revealed by in situ straining in the TEM. *Acta Mater.* **60**, 5858–5866 (2012).
27. L. Zou *et al*., Dislocation nucleation facilitated by atomic segregation. *Nat. Mater.* **17**, 56–63 (2018).
28. S. Peng, Y. Wei, Z. Jin, W. Yang, Supersonic screw dislocations gliding at the shear wave speed. *Phys. Rev. Lett.* **122**, 045501 (2019).
29. R. Peierls, The size of a dislocation. *Proc. Phys. Soc.* **52**, 34–37 (1940).
30. F. R. N. Nabarro, Fifty-year study of the Peierls-Nabarro stress. *Mat Sci. Eng. Struct.* **234**, 67–76 (1997).
31. M. J. Yao, K. G. Pradeep, C. C. Tasan, D. Raabe, A novel, single phase, non-equiatomic FeMnNiCoCr high-entropy alloy with exceptional phase stability and tensile ductility. *Scr. Mater.* **72-73**, 5–8 (2014).
32. Z. Li, K. G. Pradeep, Y. Deng, D. Raabe, C. C. Tasan, Metastable high-entropy dual-phase alloys overcome the strength-ductility trade-off. *Nature* **534**, 227–230 (2016).
33. N. L. Okamoto *et al*., Size effect, critical resolved shear stress, stacking fault energy, and solid solution strengthening in the CrMnFeCoNi high-entropy alloy. *Sci. Rep.* **6**, 35863 (2016).
34. S. Liu, Y. Wei, The Gaussian distribution of lattice size and atomic level heterogeneity in high entropy alloys. *Extreme Mech. Lett.* **11**, 84–88 (2017).
35. J. R. Rice, Dislocation nucleation from a crack tip - an analysis based on the Peierls concept. *J. Mech. Phys. Solids* **40**, 239–271 (1992).
36. S. Aubry, K. Kang, S. Ryu, W. Cai, Energy barrier for homogeneous dislocation nucleation: Comparing atomistic and continuum models. *Scr. Mater.* **64**, 1043–1046 (2011).
37. T. Zhu, J. Li, S. Yip, Atomistic study of dislocation loop emission from a crack tip. *Phys. Rev. Lett.* **93**, 025503 (2004).
38. J. R. Rice, G. E. Beltz, The activation energy for dislocation nucleation at a crack. *J. Mech. Phys. Solids* **42**, 333–360 (1994).
39. D. H. Warner, W. A. Curtin, Origins and implications of temperature-dependent activation energy barriers for dislocation nucleation in face-centered cubic metals. *Acta Mater.* **57**, 4267–4277 (2009).
40. H. Conrad, Thermally activated deformation of metals. *JOM* **16**, 582–588 (1964).
41. A. Banerjee *et al*., Ultralarge elastic deformation of nanoscale diamond. *Science* **360**, 300–302 (2018).
42. Y. Yue, P. Liu, Z. Zhang, X. Han, E. Ma, Approaching the theoretical elastic strain limit in copper nanowires. *Nano Lett.* **11**, 3151–3155 (2011).
43. H. Zhang *et al*., Approaching the ideal elastic strain limit in silicon nanowires. *Sci. Adv.* **2**, e1501382 (2016).
44. J. D. Eshelby, The determination of the elastic field of an ellipsoidal inclusion, and related problems. *Proc. R. Soc. Lond. A Math. Phys. Sci.* **241**, 376–396 (1957).
45. A. Deschamps, F. Livet, Y. Brechet, Influence of predeformation on ageing in an Al–Zn–Mg alloy—I. Microstructure evolution and mechanical properties. *Acta Mater.* **47**, 281–292 (1998).
46. H. Shercliff, M. Ashby, A process model for age hardening of aluminium alloys—I. The model. *Acta Metall. Mater.* **38**, 1789–1802 (1990).
47. F. Abe, Precipitate design for creep strengthening of 9% Cr tempered martensitic steel for ultra-supercritical power plants. *Sci. Technol. Adv. Mater.* **9**, 013002 (2008).
48. S. Plimpton, Fast parallel algorithms for short-range molecular dynamics. *J. Comput. Phys.* **117**, 1–19 (1995).
49. M. S. Daw, M. I. Baskes, Embedded atom method derivation and application to impurities, surfaces, and other defects in metals. *Phys. Rev. B Condens. Matter* **29**, 6443–6453 (1984).
50. X. W. Zhou, R. A. Johnson, H. N. G. Wadley, Misfit-energy-increasing dislocations in vapor-deposited CoFe/NiFe multilayers. *Phys. Rev. B Condens. Matter Mater. Phys.* **69**, 144113 (2004).

Downloaded at Institute of Mechanics CAS on August 31, 2020